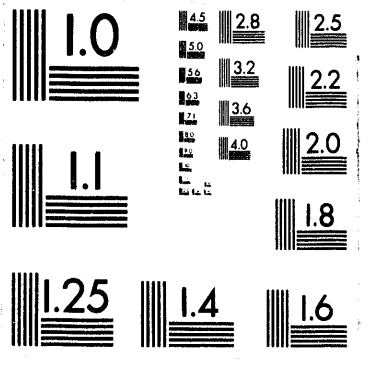
1.0
4.5
2.8
2.5
5.0
3.2
2.2
5.6
6.3
3.6
7.1
4.0
2.0
1.1
1.8
1.25
1.4
1.6

1 of 1

Conf-940692--1

LA-UR- 93-349

Title: DEVELOPEMENT OF THE AVERAGE LATTICE PHASE-STRAIN AND GLOBAL ELASTIC MACRO-STRAIN IN AL/TIC COMPOSITES

Author(s): Shi, Ning
Bourke, Mark
Goldstone, Joyce A.

Submitted to: ICRS-4

RECEIVED
FEB 07 1994
OSTI

MASTER

DISCLAIMER

This report was prepared as an account of work sponsored by an agency of the United States Government. Neither the United States Government nor any agency thereof, nor any of their employees, makes any warranty, express or implied, or assumes any legal liability or responsibility for the accuracy, completeness, or usefulness of any information, apparatus, product, or process disclosed, or represents that its use would not infringe privately owned rights. Reference herein to any specific commercial product, process, or service by trade name, trademark, manufacturer, or otherwise does not necessarily constitute or imply its endorsement, recommendation, or favoring by the United States Government or any agency thereof. The views and opinions of authors expressed herein do not necessarily state or reflect those of the United States Government or any agency thereof.

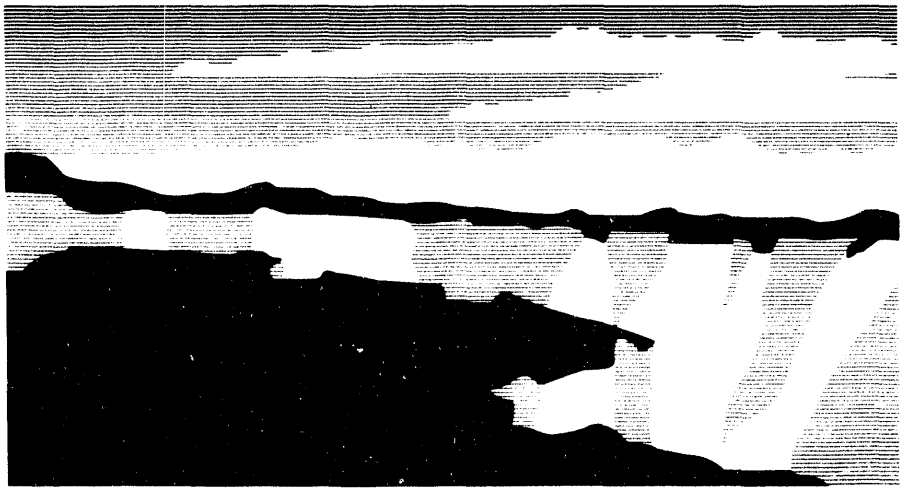

Los Alamos
NATIONAL LABORATORY

Los Alamos National Laboratory, an affirmative action/equal opportunity employer, is operated by the University of California for the U.S. Department of Energy under contract W-7405-ENG-36. By acceptance of this article, the publisher recognizes that the U.S. Government retains a nonexclusive, royalty-free license to publish or reproduce the published form of this contribution, or to allow others to do so, for U.S. Government purposes. The Los Alamos National Laboratory requests that the publisher identify this article as work performed under the auspices of the U.S. Department of Energy.

Form No. 836 R5
ST 2629 10/91

DISTRIBUTION OF THIS DOCUMENT IS UNLIMITED

DEVELOPMENT OF THE AVERAGE LATTICE PHASE-STRAIN AND GLOBAL ELASTIC MACRO-STRAIN IN AL/TIC COMPOSITES

N. SHI[1], M. A. M. BOURKE[1], J. A. GOLDSTONE[1] AND J. E. ALLISON[2]
[1]LOS ALAMOS NATIONAL LABORATORY
LOS ALAMOS, NM 87545
[2]FORD MOTOR CO.
DEARBORN, MI 48121

ABSTRACT

The development of elastic lattice phase strains and global elastic macro-strain in a 15 volume percent (V%) TiC particle reinforced 2219-T6 Al composite was modeled by finite element method (FEM) as a function of tensile uniaxial loading. The numerical predictions are in excellent agreement with strain measurements at a spallation neutron source. Results from the measurements and modeling indicate that the lattice phase-strains go through a "zigzag" increase with the applied load in the direction perpendicular to the load, while the changes of slope in the parallel direction are monotonic. FEM results further showed that it is essential to consider the effect of thermal residual stresses (TRS) in understanding this anomalous behavior. It was demonstrated that, due to TRS, the site of matrix plastic flow initiation changed. On the other hand, the changes of slope of the elastic global macrostrain is solely determined by the phase-stress partition in the composite. An analytical calculation showed that both experimental and numerical slope changes during elastic global strain response under loading could be accurately reproduced by accounting for the changes of phase-stress ratio between the matrix and the matrix.

INTRODUCTION

Thermal residual stresses (TRS) have been under intense investigation in a variety of composites for several years (e.g. [1–6]). They result from differences in the coefficient of thermal expansion (ΔCTE) between the constituent phases during cooling. Recent investigations indicate that TRS has a profound influence on the mechanical behavior of metal matrix composites (MMCs) [7–14]. It has been suggested that the matrix plastic flow in MMCs is strongly influenced by the TRS [10, 13, 15], and that this influence is responsible for the observed asymmetric composite constitutive behavior between tension and compression [8,10–12,14]. Dislocations induced by plastic relaxation of thermal stresses during cooling may result in significant strengthening [7, 9]. Deformation-induced changes of residual stresses have also been extensively studied [16, 17]. These changes in residual stress have been found to affect the material performance under complex loading histories. For example, under cyclic loading such as a Bauschinger test, residual stresses polarize the yielding stresses in the two opposing loading cycles [18, 19].

The evolution of lattice elastic phase-strain under a uniaxial load is important in studying the changes of stress distribution in composites. Since phase-stresses are *linearly* related to the elastic lattice phase-strains, when redistributions of local field quantities (e.g. stress and strain) do not occur, the lattice phase-strain increases linearly with the applied load irrespective of the state deformation, i.e. either elastic or plastic. Therefore, any deviation from linearity indicates stress redistribution in the composite, commonly referred to as a load transfer, which is important for the strengthening of composites.

Recently, Allen *et al.* measured *in situ* load-induced lattice elastic phase-strains in Al/SiC particulate- and whisker-reinforced composites using neutron diffraction [20]. This technique enables a direct observation of the responses from individual phases under load. They found that diffusion stress relaxation is an important mechanism in understanding the responses of the load-induced lattice strains. However, the influence of TRS on the evolution of elastic phase-strain has never been studied in detail.

For any ductile solid, the total strain (ε^{total}) under static loading consists of elastic (ε^{e}) and plastic (ε^{pl}) components, *i.e.*, $\varepsilon^{total} = \varepsilon^{e} + \varepsilon^{pl}$. The elastic strain is completely recoverable while the plastic component is a measure of permanent distortion. For a single phase material, the global elastic strain component is *always* linearly related to the applied load, and will be

completely recovered upon unloading. The unrecoverable strain component after unloading, ϵ^{pmt}, is defined as the plastic strain (ϵ^{pl}). This is the strain component resulting, ideally, from material flow in addition to the elastically stretching of the lattice.

In a multiphase material in which the mechanical properties of each phase are different, a similar global elastic strain behavior is usually assumed, i.e. the global elastic strain component is linearly related to the applied load. However, experimental observations of the evolution of the load-induced global elastic strain component during elasto-plastic deformation have not been made, and its implications not been carefully studied.

Neutron diffraction is a suitable technique for measuring elastic lattice phase-strains in MMCs. It has a greater penetration depth than x-rays. For example, the penetration depth differs by approximately 3 orders of magnitude in Al. In contrast to the more commonly available reactor sources, neutrons from a spallation source offer advantages by virtue of their production in a series of discrete pulses. Using time of flight (TOF), a unidirectional strain component can be determined from the changes of lattice spacing from all possible diffracting planes in one measurement.

In this investigation, the evolution of lattice phase-strain and elastic global strain under uniaxial tensile loading of a particle-reinforced Al/TiC composite was studied. A numerical analysis was performed using the finite element method (FEM) to model the influence of TRS on the evolution of the lattice elastic phase-strains both parallel and perpendicular to the loading direction. The correlation between the phase-stress partition and the global elastic strain was investigated. The results were compared with the neutron diffraction measurements obtained using a compact stress rig at the Manuel Lujan, Jr. Neutron Scattering Center (LANSCE) of Los Alamos National Laboratory.

EXPERIMENTAL BACKGROUND

The material used in this study was a 2219 Al alloy reinforced with 15 volume percent (V%) TiC particles. The average diameter of the reinforcement was about 3 μm [21]. The composite was produced *in situ* by Martin Marietta using the XD^{TM} process. The as-received composite was first rolled into plates, heat treated in T6 condition, then machined into a standard cylindrical tensile test specimen with a gauge length and diameter of 12.27 and 1.0 cm, respectively. The gauge length was arbitrarily selected for a free passage of the neutron beam without interference from the grips.

During diffraction measurements, lattice strains were measured as a function of applied uniaxial tensile load. A gauge length of 1.4 cm was illuminated by the neutron beam corresponding to a total irradiated volume of 1.1 cm^3. Initially, a tensile load of 200 MPa was applied, followed by unloading, to detect modifications of residual strain induced by a small load. Then, the specimen was incrementally loaded to 327 MPa sufficient to induce 1% total strain as recorded by a strain gauge attached to the specimen. The loading results in a total plastic strain of 0.67% upon unloading. The loading process was divided into intervals of approximately 50 MPa. During each measurement, the specimen was controlled at a constant cross-head displacement. Lattice strains, both parallel and perpendicular to the loading direction, were measured from both phases. Each measurement took approximately 5 hrs, during which, the stress relaxation was less than 1% except near the maximum stress level (> 300 MPa), at which 1.5% reduction in stress was detected by the load cell.

Strains determined from individual lattice reflection may be affected by the matrix texture [22, 23]. To minimize the effect of texture, we employed the Rietveld profile refinement, which entails a fit of all the lattice reflections to give a global lattice parameter that responds to the applied load based on the collective behavior from all lattice planes [24].

FEM MODELING

The composite was assumed to be an infinite three dimensional (3-D) cubic array of periodically distributed cubic particles embedded in the matrix with volume fraction of 15 V%. By invoking symmetry, an equivalent unit cell may be used where a standard periodic boundary condition was employed [25]. Tests with spherical and cubic particle shapes were performed. The difference in the responses of the *average* elastic phase-strain between the two particle morphologies was not significant. As compared with spherical particles, cubic particles induce stress concentrations near the particle corners. However, the stress concentration is localized. The effect is averaged out in a volume-weighted averaging process, which is required for comparison with the diffraction results. For simplicity, we choose to report the cubic results.

Another approach to simplify the geometry of the problem is to consider the reinforcements as a cubic array of equi-axial cylinders and construct the unit cell as an axisymmetric cylinder. Although the material continuity is sacrificed at the cell boundary, the unit cell is axisymmetric which can be reduced to a 2-D model for calculation. This technique has been used extensively, (e.g. [17]). In this analysis, both axisymmetric and 3-D calculations were made. The composite bulk responses

of elastic phase-strain were modeled by the 3-D unit cell model. For the evolution of the local matrix plastic flow, the axisymmetric model was used, for it is much simpler to display the distribution of the field quantities in 2-D. Figure 1 displays the composite stress–strain curves predicted by these two models. Only small difference can be detected.

During FEM analysis, the TiC was assumed to be elastic throughout the loading process, and the Al matrix followed the elastic/linear-plastic bilinear stress–strain relationship and the isotropic-hardening rule. The Von Mises yielding criterion was used. The material properties were obtained from [26, 27]. Average lattice phase-strains were approximated by a volume-average of the elastic component of the total strains. The mesh size was chosen when the dependency of the generated stress–strain curve was negligible on the mesh-size refinement. Time-dependent deformation was not incorporated in the analysis so that the effect of creep-type stress relaxation was not considered.

INFLUENCE OF TRS ON THE EVOLUTION OF LATTICE PHASE-STRAIN

To understand the impact of TRS, two different loading histories were examined. In the first case (History I), the composite was assumed to be stress free at 200°C. A total temperature drop of 180°C was uniformly applied in steps to all the nodal points in the FEM mesh. After the cooling, a tensile uniaxial load was applied incrementally along the x_2 direction. To model the loading history employed in the experiment, the following sequence was applied: $0 \Rightarrow 200 \Rightarrow 0 \Rightarrow 327 \Rightarrow 0$ MPa. The FEM results indicated that the initial loading, $0 \Rightarrow 200 \Rightarrow 0$ MPa, had little influence on the subsequent composite stress–strain responses. To compare with a hypothetical composite devoid of the influence of TRS, a separate second loading scheme (History II) was employed, which did not include the cooling history, and the initial loading cycle of 200 MPa was ignored, for it gave little difference. Figure 2 displays the stress–strain curve generated by the FEM under History I and the experimental stress–strain values at which the diffraction measurements were taken.

Phenomenological Responses of the Lattice Elastic Strain

The FEM results under the History I are shown in Fig. 3 along with the diffraction profile refinement data. Excellent agreement was achieved between the prediction and the experiment. Along the perpendicular direction, as the average elastic strain in the *particle* increased, the *magnitude* of the slope of this increase became larger prior to the composite global yielding, and smaller as the composite started to macroscopically yield [Fig. 3(a)]. On the perpendicular *matrix* elastic strain, an opposite trend was observed. The *magnitude* of the slope decreased with an increasing load before a final increase upon global yielding [Fig. 3(b)]. This behavior may be characterized as a "zigzag" increase, i.e. the changes of the slope were nonmonotonic. This zigzag behavior may be best viewed through the three representative stages as defined in Fig. 3(b) distinguished by their slopes.

In the parallel direction, on the other hand, the behavior of elastic strains in both phases was different from that of the perpendicular strains. For a given amount of matrix lattice strain increase, the corresponding changes of the stress reduced as the load increased.

To assess the influence of the TRS on the morphology of the strain variations, the History II was implemented, where the effect of ΔCTE was not considered. Figure 4 displays the predicted increases of elastic lattice strains as a function of the applied stress, where the applied stress extends to 350 MPa to reveal clearer effects of a full matrix plasticity. The material thermal history had a significant impact on the morphology of the elastic lattice phase-strain response as compared with Fig. 3. The changes of slope of the elastic lattice strains in both phases were monotonic in the perpendicular direction [Fig. 4(a)], while those parallel to the loading direction were nonmonotonic (i.e. "zigzag increases") [Fig. 4(b)]. These differences as a result of excluding the effect of ΔCTE indicate that TRS is important in understanding the phenomenological responses of the lattice elastic strain.

Matrix Plastic Flow

To further study the influence of the TRS and understand the origin of the morphology of the phenomenological response of the lattice phase-strain, the evolution of the matrix plastic flow was investigated through a 2-D axisymmetric FEM model. It was shown that plastic flow first initiated at the side of the particle, and propagated toward the top of the particle as the applied load increased. Figure 5(a) shows the effective plastic strain contours ($\bar{\varepsilon}^p = \sqrt{\frac{2}{3}\varepsilon^p_{ij}\varepsilon^p_{ij}}$) of the matrix at an applied load of 270 MPa under the History I, showing the initiation of the matrix plastic flow.

When TRS was not considered (History II), the development of the matrix plastic different. The matrix start to flow at the top of the particle to compensate the rigidity of the particle. As shown in Fig. 5(b), in contrast with the History I, a large

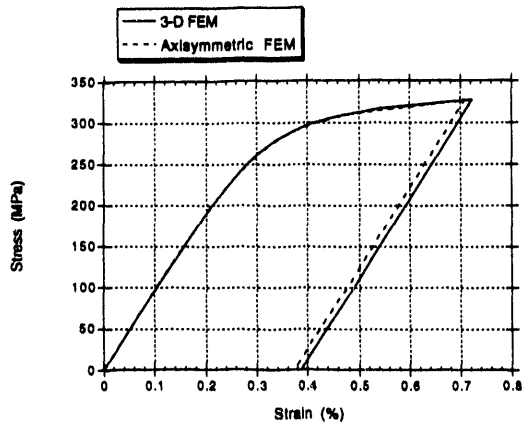

Figure 1: A comparison of the stress-strain curves predicted by the axisymmetric and the 3-D FEM models.

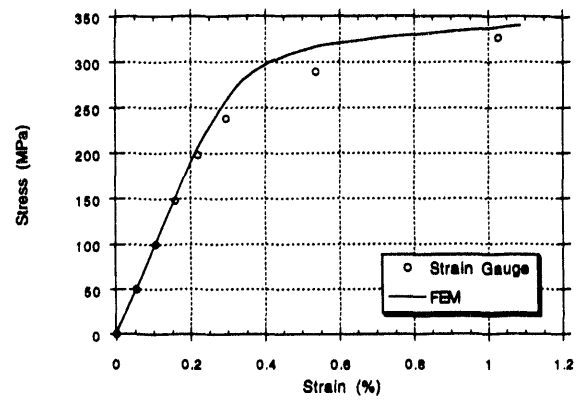

Figure 2: Stress-strain curve predicted by the FEM following the History I where the thermal history is considered. The open circles are the experimentally measured stress-strain values recorded by the strain gauge.

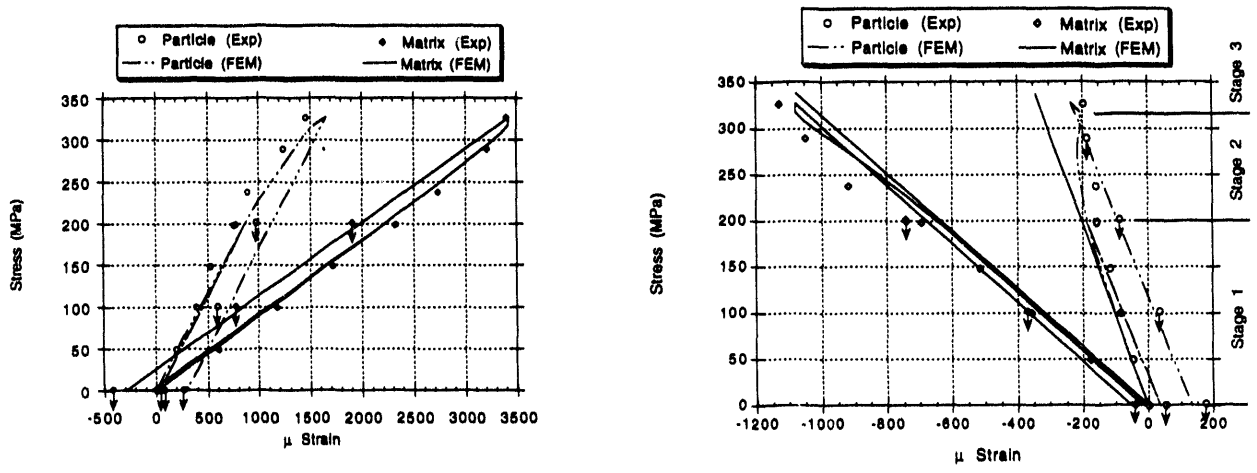

Figure 3: Comparisons of the evolution of the lattice phase-strain predicted by the FEM under the first loading scheme (History I) and the Rietveld profile refinement of the diffraction data, where data points with arrows are from unloading; (a) parallel strains are shown, the changes of the slope are monotonic; (b) perpendicular strains are shown. The changes of slope are nonmonotonic ("zigzag"). The straight lines are references to show the "zigzagging." The three stages are defined based on the changes of slope.

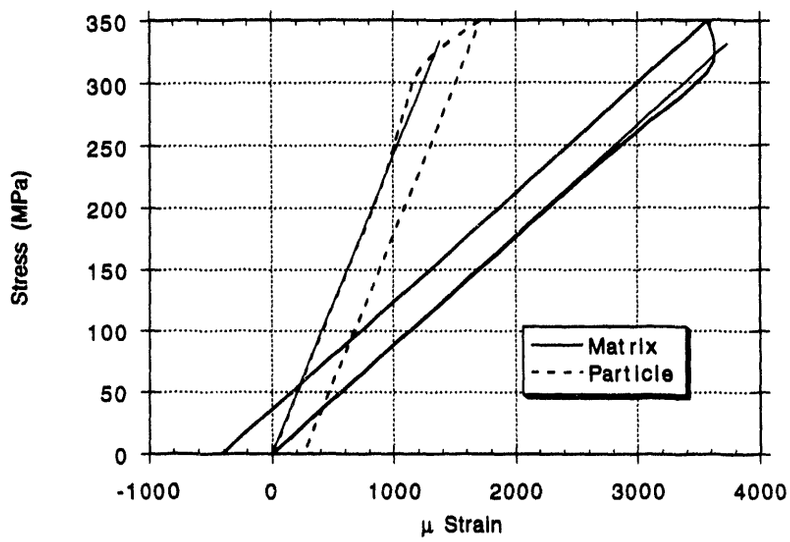

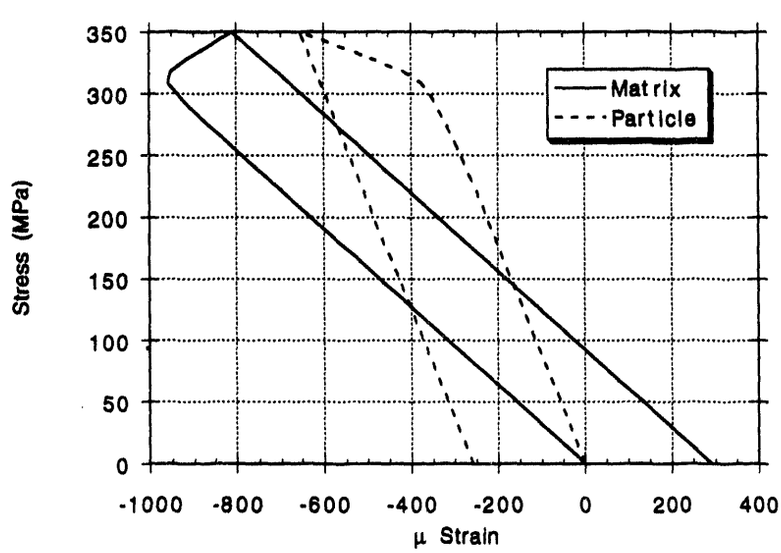

Figure 4: Lattice phase-strains predicted by the FEM following the second loading scheme (History II) where the thermal history is not considered; (a) parallel strains are shown, the changes of the slope are nonmonotonic ("zigzag"), the straight lines are references to show the "zigzagging;" (b) perpendicular strains are shown, the changes of the slope monotonic.

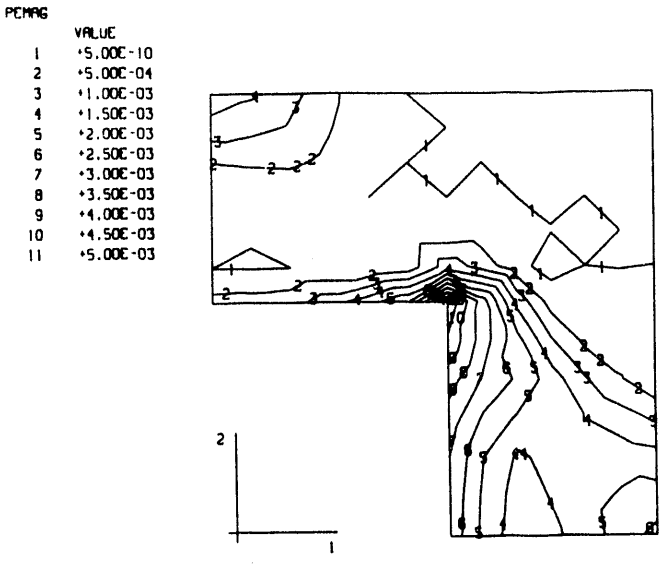

ALTIC AT P=270MPA

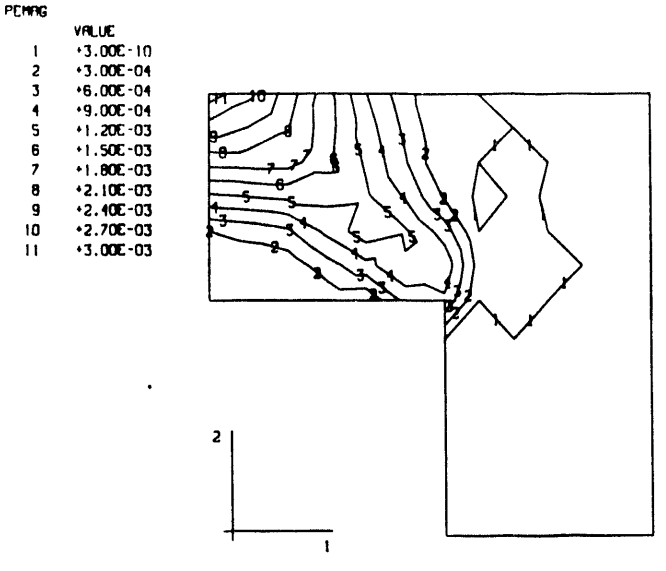

ALTIC AT P=270MPA W/O COOLING

Figure 5: Effective plastic strain contours at applied load of 270 MPa; (a) when the thermal history is considered; (b) when the thermal history is not considered.

plastic flow gradient appeared at the top of the particle under the same applied load level (270 MPa), whereas the rest of the matrix remained elastic.

By comparing the plastic flow initiation shown in Figs. 5(a) and 5(b), it is evident that a major influence of TRS is to dominate the location of the plastic flow initiation. With initial TRS, the plastic flow starts at the side of the particle, whereas, if the composite is TRS-free, the initiation of matrix plastic flow occurs at the top of the particle. The shift of plastic flow initiation site due to TRS causes the observed zigzag elastic phase-strain evolution.

GLOBAL ELASTIC MACRO-STRAIN AND PHASE-STRESS PARTITION

For displacements along the boundary of a domain D, the following expression can be obtained from Guass's theorem:

$$\int_D \partial_k u_i \delta_{jk} dD = \int_{|D|} u_i \delta_{jk} n_k dS, \tag{1}$$

where u_i is the displacement along the ith direction, and x_j is the coordinate in the jth direction. The $|D|$ is the boundary of the volume D. The repeated subscript indices are summed over 1, 2 and 3. The ∂_k denotes a partial derivative over x_k. When $i = j$, the normal strains in the integrated volume D are related to the far-field displacement u_i by Eq. 1. In reality, the global strain (e.g. of a tensile bar) may be obtained by dividing the far-field displacement by the sample overall dimension, and be related to the internal strains by Eq. 1.

For normal phase-strains in a two-phase material, the following mean-field expressions may be obtained from Eq. 1:

$$(1-f)\langle\varepsilon\rangle_m + f\langle\varepsilon\rangle_r = \bar{\varepsilon}, \tag{2}$$

where f is the volume fraction of the reinforcement. The ε denotes the normal strain. The carats "$\langle\ \rangle$" imply averages over the appropriate volume. The "$\bar{\ }$" represents corresponding average of the far-field quantities over the appropriate boundary. In the remainder of this paper, the $\bar{\sigma}$ and $\bar{\varepsilon}$ represent the far-field stress and the global strain derived from the far-field displacement, respectively. The subscripts "m" and "r" stand for the matrix and reinforcement, respectively. Equation 2 indicates that the global normal strain can be readily related to the material phase-strains by a simple volume averaging rule. For displacement induced by the elastic strain component, Equations 1 and 2 also apply. That is, the global elastic strain component can be obtained by an volume-average of the elastic phase-strains, as in Eq. 2.

The global strains obtained from neutron diffraction through Eq. 2 is nonlinear with the applied load (squares in Figure 6). This is contrary to the behavior of a monolithic material. To understand this interesting characteristic, we need to consider the plastic deformation process in a multiphase material. When a composite plastically deforms, the proportion of the load shared by the stiffer reinforcement increases [20, 25]. Therefore, it is logical to investigate the correlation between the changes of load sharing and the slope changes.

During loading, every increment of applied stress, $\Delta\bar{\sigma}_{ij}$, invokes internal stress partition between the two phases in a composite. This may be given by [28]

$$(1-f)\Delta\langle\sigma_{ij}\rangle_m + f\Delta\langle\sigma_{ij}\rangle_r = \Delta\bar{\sigma}_{ij}, \tag{3}$$

where $\Delta\sigma_{ij}$ are the stress increments. For a spherical composite with loading along x_3, the average normal stresses along the axes of the global coordinates are the principle average stresses ($\langle\sigma_i\rangle$, $i = 1$, 2 or 3). If we formulate a ratio of the increments of reinforcement and matrix stresses ($R = \Delta\langle\sigma_i\rangle_r / \Delta\langle\sigma_i\rangle_m$), this ratio can be used as a measure of the internal phase-stress partition or the load sharing. To express in a tensor form, we have

$$\tilde{R} = \Delta\tilde{\sigma}_r \Delta\tilde{\sigma}_m^{-1} = \tilde{C}_r \Delta\tilde{\varepsilon}_r^e (\Delta\tilde{\varepsilon}_m^e)^{-1} \tilde{C}_m^{-1} \tag{4}$$

where $\tilde{C}$ is the stiffness tensor; the $\Delta\tilde{\sigma}$ and $\Delta\tilde{\varepsilon}^e$ are the increments of the average stress and elastic strain tensors, respectively; the $\tilde{R}$ is the tensor of the load sharing ratio, where the tilde "$\tilde{\ }$" denotes a tensor quantity. In $\tilde{R}$, only the diagonal elements are non-zero, and they are functions of both the material properties and the stresses.

Considering Eqs. 2 and 3, we can obtain the following by substitution of Eq. 4:

$$\Delta\tilde{\bar{\sigma}} = [\tilde{I} + f(\tilde{R} - \tilde{I})]\Delta\tilde{\sigma}_m; \tag{5}$$

$$\Delta\tilde{\bar{\varepsilon}}^e = [\tilde{I} + f(\tilde{C}_r^{-1}\tilde{R}\tilde{C}_m - \tilde{I})]\Delta\tilde{\varepsilon}_m^e. \tag{6}$$

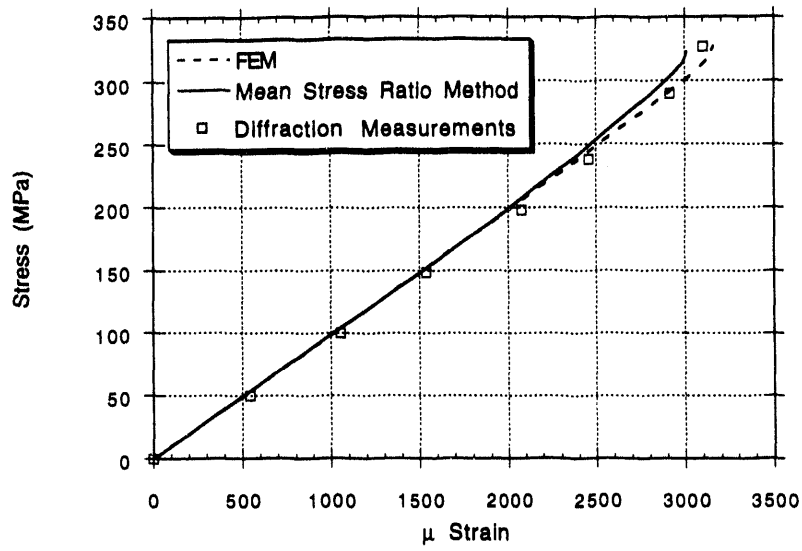

Figure 6: Evolution of the global elastic strain component obtained from diffraction, FEM, and Eq. 8.

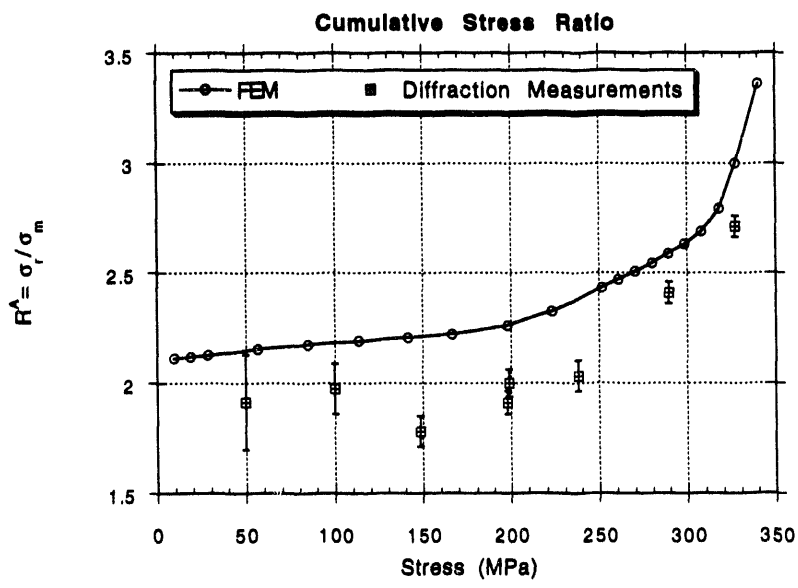

Figure 7: Changes of the phase-stress ratio between the particles and the matrix as a function of the applied load from both diffraction and FEM.

Notice that the tangent modulus along the loading direction, "L^t_{33}", of the stress–elastic-strain curve in Fig. 6 is defined as $L^t_{33} = \frac{\Delta\sigma_{33}}{\Delta\tilde{\epsilon}^e_{33}}$. By considering Eqs. 5 and 6, we may get

$$\tilde{L}^t = \Delta\tilde{\sigma}(\Delta\tilde{\epsilon}^e)^{-1} = [\tilde{I} + f(\tilde{R} - \tilde{I})]\tilde{C}_m[\tilde{I} + f(\tilde{C}_r^{-1}\tilde{R}\tilde{C}_m - \tilde{I})]^{-1} \tag{7}$$

where $\tilde{L}^t$ is the tensor of tangent moduli of the composite in the stress–elastic-strain relationship. Using the reduced indices notation, the tangent modulus of the elastic strain curve along x_3 direction is

$$L^t_{33} = \frac{(\lambda_m + 2G_m)[1 + f(R_{33} - 1)]}{1 + f\left[\frac{R_{33}}{E_r}(\lambda_m + 2G_m) - 1\right]} \tag{8}$$

where λ is the Lame's constant, the G and E are the shear and Young's moduli. Taking derivative with respect to R_{33}, we obtain

$$\frac{\partial L^t_{33}}{\partial R_{33}} = \frac{f(1-f)(\lambda_m + 2G_m)\left(1 - \frac{\lambda_m + 2G_m}{E_r}\right)}{\left[1 + f\left(\frac{\lambda_m + 2G_m}{E_r}R_{33} - 1\right)\right]^2} \tag{9}$$

In Eq. 9, the derivative, $\frac{\partial L^t_{33}}{\partial R_{33}}$, is positive ($> 0$) when E_r/E_m is approximately larger than 0.5. That is, the tangential stiffness, L^t_{33}, increases with the load sharing ratio, R, for composites with the stiffness of the inclusions at least 50% of that of the matrix. The $\tilde{L}^t$ becomes secant moduli when $\tilde{R}$ is taken as the *cumulative* phase-stress ratio. Figure 6 displays the evolution of the global elastic strain deduced from Eq. 8 in which the cumulative phase-stress ratio at a corresponding load level is obtained from FEM. The global elastic strains as a function of the applied load obtained from FEM and neutron diffraction are also shown. A very good agreement with the measurement is obtained. The slope change in Fig. 6 can best be explained by the fact that the reinforcement in a composite takes more load when plastic flow starts in the matrix. Figure 7 shows the cumulative phase-stress ratio obtained from FEM and neutron diffraction.

There is an important implication on the one-to-one correspondence between the load partition "$\tilde{R}$" and the tangent moduli "$\tilde{L}^t$" in Eq. 8. The load sharing ratio, R, between the reinforcement and the matrix increases as the matrix in a composite starts to plastically deform, while it decreases upon particle fracture and interfacial debonding. Therefore, these two processes are distinct during the evolution of the global *elastic* strain component. In contrast, for the development of *total* strain during a simple tensile test, the contributions from both processes are similar. They make the material more compliant. Therefore, when supplemented by proper micro-analyses, this characteristic is potentially important in identifying the onset of particle fracturing during plastic deformation.

CONCLUSIONS

From this work, the following conclusions can be made for the present Al/TiC composite:

(1) Good agreement has been achieved between the diffraction data and the FEM modeling on both the average elastic phase-strain and the global elastic macro-strain.

(2) The slope changes in the load-induced lattice phase-strain are nonmonotonic in the perpendicular direction, while they are monotonic in the parallel direction. The FEM model indicates that this anomalous behavior of lattice phase-strain response can best be predicted by considering the effects of TRS. The TRS induces plastic flow in the matrix near the parallel particle–matrix interface, while, in a composite devoid of TRS, the matrix plastic flow initiates near the perpendicular particle–matrix interface.

(3) The slope changes the global elastic macro-strain follow the same trend as the changes of the load sharing ratio between the reinforcement and the matrix. There is an one-to-one correspondence between the phase-stress ratio and the tangent modulus in the stress–elastic-strain relationship.

Acknowledgements—LANSCE is a national user facility funded by the United States Department of Energy, Office of Basic Energy Science. This work was supported in part by DOE contract W7405-ENG-36. The authors would like to thank D. Davis, G. Baker and M. Lovato who were involved in the design of the stress rig; A. C. Lawson and M. G. Stout for their technical support during diffraction measurement; and J. Lasecki, G. Vyletel and P. Krajewski who prepared the samples. NS would like to acknowledge F. Guerra and P. Goldman for making ABAQUS FE Code available, and R. B. Schwarz for his encouragement.

References

[1] H. M. Ledbetter and M. W. Austin, *Mater. Sci. Engng* **89**, 53 (1987).

[2] A. D. Krawitz, D. G. Reichel and R. L. Hitterman, *Mater. Sci. Engng* **A119**, 127 (1989).

[3] B. Eigenmann, B. Scholtes and E. Macherauch, *Mater. Sci. Engng* **A118**, 1 (1989).

[4] S. Majumdar, J. P. Singh, D. S. Kupperman and A. D. Krawitz, *J. Engng Mater. Tech.* **113**, 51 (1991).

[5] L. F. Smith, A. D. Krawitz, P. Clark, S. Saimoto, N. Shi and R. J. Arsenault, *Mater. Sci. Engng* **A159**, L13 (1992).

[6] M. A. M. Bourke, J. A. Goldstone and T. M. Holden, in *Measurement of Residual and Applied Stress Using Neutron Diffraction* (ed. by M. T. Hutchings and A. D. Krawitz), p. 369-382. Kluwer Acd. Pub., Netherland (1992).

[7] R. J. Arsenault and N. Shi, *Mater. Sci. Engng* **81**, 175 (1986).

[8] R. J. Arsenault and M. Taya, *Acta metall.* **35**, 651 (1987).

[9] M. Taya, K. E. Lulay and D. J. Lloyd, *Acta metall. mater.* **39**, 59 (1991).

[10] A. Levy and J. M. Papazian, *Acta metall. mater.* **39**, 2255 (1991).

[11] P. J. Withers, W. M. Stobbs and O. B. Pedersen, *Acta metall.* **37**, 3061 (1989).

[12] N. Shi and R. J. Arsenault, *J. Comp. Tech. Res.* **13**, 211 (1991).

[13] N. Shi, B. Wilner and R. J. Arsenault, *Acta metall. mater.* **40**, 2841 (1992).

[14] N. Shi and R. J. Arsenault, *Scripta metall. mater.* **27**, 623 (1993).

[15] N. Shi and R. J. Arsenault, *Ann. Rev. Mater. Sci.* (ed. R. A. Huggins, J. A. Giordmaine and J. B. Watchman, Jr.) vol. 24, Ann. Rev. Inc., CA (1994), to be published.

[16] N. Shi, R. J. Arsenault, A. D. Krawitz and L. F. Smith, *Metall. Trans.* **24A**, 187 (1993).

[17] G. L. Povirk, M. G. Stout, M. A. M. Bourke, J. A. Goldstone, A. C. Lawson, M. Lovato, S. R. Nutt and A. Needleman, *Acta metall. mater.* **40**, 2391 (1992).

[18] R. J. Arsenault and S. B. Wu, *Mater. Sci. Engng* **96**, 77 (1987).

[19] N. Shi and R. J. Arsenault, *Metall. Trans.* **24A**, 1879 (1993).

[20] A. J. Allen, M. A. M. Bourke, S. Dawes, M. T. Hutchings and P. J. Withers, *Acta metall. mater.* **40**, 2361 (1992).

[21] G. M. Vyletel, D. C. Van Aken and J. E. Allison, *Scripta metall. mater.* **25**, 2405 (1991).

[22] M. A. M. Bourke, J. A. Goldstone, N. Shi, J. E. Allison, M. G. Stout and A. C. Lawson, *Scripta metall. mater.* **29**, 771 (1993).

[23] M. A. M. Bourke, J. A. Goldstone, M. G. Stout, A. C. Lawson and J. E. Allison, in *Proceeding of the 122nd TMS Annual Meeting* (edited E. V. Barrera and I. Dutta), pp. 67. TMS, PA (1993).

[24] R. B. Von Dreele, J. D. Jorgenen, and C. G. Windsor, *J. Appl. Crystallogr.* **15**, 581 (1982).

[25] N. Shi, M. A. M. Bourke, J. A. Goldstone and J. E. Allison, submitted for publication.

[26] *Metals Handbook, Vol. 2—Properties and Selection: Nonferrous Alloys and Pure Metals.* ASM, Ohio (1979).

[27] *The CRC Material Science and Engineering Handbook* (ed. by J. Shackelford and W. Alexander). CRC Press, Florida (1992).

[28] T. Mura, *Micromechanics of Defects in Solids*, 2nd edn., Martinus Nijhoff, the Hague, 1987.

DATE
FILMED
5/10/94

END